Low Cloud Type over the Ocean from Surface Observations. Part III: Relationship to Vertical Motion and the Regional Surface Synoptic Environment

JOEL R. NORRIS

National Center for Atmospheric Research, Boulder, Colorado*

STEPHEN A. KLEIN

Geophysical Fluid Dynamics Laboratory, NOAA, Princeton University, Princeton, New Jersey

(Manuscript received 30 June 1998, in final form 11 January 1999)

ABSTRACT

Composite large-scale dynamical fields contemporaneous with low cloud types observed at midlatitude Ocean Weather Station (OWS) C and eastern subtropical OWS N are used to establish representative relationships between low cloud type and the synoptic environment. The composites are constructed by averaging meteorological observations of surface wind and sea level pressure from volunteering observing ships (VOS) and analyses of sea level pressure, 1000-mb wind, and 700-mb pressure vertical velocity from the National Centers for Environmental Prediction–National Center for Atmospheric Research (NCEP–NCAR) reanalysis project on those dates and times of day when a particular low cloud type was reported at the OWS.

VOS and NCEP results for OWS C during summer show that bad-weather stratus occurs with strong convergence and ascent slightly ahead of a surface low center and trough. Cumulus-under-stratocumulus and moderate and large cumulus occur with divergence and subsidence in the cold sector of an extratropical cyclone. Both sky-obscuring fog and no-low-cloud typically occur with southwesterly flow from regions of warmer sea surface temperature and differ primarily according to slight surface convergence and stronger warm advection in the case of sky-obscuring fog or surface divergence and weaker warm advection in the case of no-low-cloud. Fair-weather stratus and ordinary stratocumulus are associated with a mixture of meteorological conditions, but differ with respect to vertical motion in the environment. Fair-weather stratus occurs most commonly in the presence of slight convergence and ascent, while stratocumulus often occurs in the presence of divergence and subsidence.

Surface divergence and estimated subsidence at the top of the boundary layer are calculated from VOS observations. At both OWS C and OWS N during summer and winter these values are large for ordinary stratocumulus, less for cumulus-under-stratocumulus, and least (and sometimes slightly negative) for moderate and large cumulus. Subsidence interpolated from NCEP analyses to the top of the boundary layer does not exhibit such variation, but the discrepancy may be due to deficiencies in the analysis procedure or the boundary layer parameterization of the NCEP model. The VOS results suggest that decreasing divergence and subsidence in addition to increasing sea surface temperature may promote the transition from stratocumulus to trade cumulus observed over low-latitude oceans.

1. Introduction

Low clouds over subtropical and midlatitude oceans are an important part of the climate system because their relatively high albedo can greatly reduce the net radiation absorbed by the ocean (Slingo 1990). Many studies have been undertaken to understand factors controlling marine boundary layer (MBL) cloud amount and cloud optical properties. These include aircraft observations of cloud properties, MBL structure, and MBL processes over subtropical and midlatitude oceans (e.g., Albrecht et al. 1988, 1995; Boers et al. 1998a; Nicholls and Leighton 1986; Smith and Jonas 1995). Other investigations have documented relationships between cloud amount, cloud optical thickness, cloud radiative forcing, and large-scale parameters such as sea surface temperature (SST), lower-tropospheric static stability, horizontal advection, and vertical motion (e.g., Klein and Hartmann 1993; Klein et al. 1995; Norris et al. 1998; Lau and Crane 1997; Weaver and Ramanathan 1997).

These studies have greatly increased our understanding of many aspects of low cloudiness over the ocean, but some cloud types, MBL structures, and meteorological situations have received less attention. Aircraft

* The National Center for Atmospheric Research is sponsored by the National Science Foundation.

Corresponding author address: Joel R. Norris, GFDL/NOAA, Princeton University, P.O. Box 308, Princeton, NJ 08542.
E-mail: jnorris@ucar.edu

observations have focused almost exclusively on stratocumulus and cumulus in inversion-capped convective MBLs even though nonconvective stratus and nonconvective fog are common at midlatitudes. Large-scale investigations have generally used broad categories of cloudiness, which hinder examination of relationships between cloud properties and specific MBL conditions. Additional investigation into how cloud properties are related to MBL structure and the synoptic environment is needed for all types of clouds, particularly at midlatitudes. Knowledge of the typical synoptic environments, which generally accompany various cloud types would help direct future field experiments to the cloud type and MBL condition they would like to observe. This knowledge would also be useful for comprehensively evaluating cloud and turbulence schemes and MBL structure in large-scale models (e.g., Martin et al. 1999, manuscript submitted to *Mon. Wea. Rev.*).

Norris (1998a) used coincident soundings and surface meteorological observations from four Ocean Weather Stations (OWS) to document relationships between low cloud type, MBL structure, and local surface meteorology at substantially different geographical locations and seasons. Norris (1998b) used a global dataset of synoptic surface cloud observations primarily made by volunteer observing ships (VOS) to document how climatological distributions of low cloud type frequency were related to climatological patterns of MBL structure, advection, surface divergence, and synoptic activity over the global ocean. These previous studies addressed typical MBL structures associated with low cloud types but could not examine typical vertical motion associated with them because only data at a single location (hence preventing the calculation of divergence) or climatological data were used. The present paper, the third in this series, addresses this aspect of the problem by documenting the vertical motion and regional surface synoptic environment associated with various cloud types. This is done by averaging onto a grid all VOS meteorological observations in the region reported at the same time as a particular low cloud type was observed by an OWS. Output from the National Centers for Environmental Prediction–National Center for Atmospheric Research (NCEP–NCAR) reanalysis project (Kalnay et al. 1996) is averaged as well.

Regional composites of surface wind and sea level pressure (SLP) from VOS observations and from NCEP analyses are presented for bad-weather stratus, fair-weather stratus, stratocumulus, cumulus-under-stratocumulus, moderate and large cumulus, sky-obscuring fog, and no-low-cloud observed at OWS C in the western midlatitude North Atlantic during summer. Surface divergence of the wind field composited from the VOS observations and pressure vertical velocity (ω) at 700 mb from NCEP analyses are used to show the distribution of vertical motion associated with the low cloud types. OWS C was chosen as the center point for the regional composites because it has a midlatitude location, because it is in the region of the global ocean with the highest density of VOS observations, and because Norris (1998a) presented many composite soundings for low cloud types at OWS C. Surface divergence and 700-mb ω at OWS C during winter and OWS N in the eastern subtropical North Pacific are also documented.

TABLE 1. Low cloud types examined in this study.

C_L Code	Low cloud type
0	No-low-cloud
1	Small cumulus (small Cu)
2	Moderate and large cumulus (Cu)
5	Ordinary stratocumulus (Sc)
6	Fair-weather stratus (St)
7	Bad-weather stratus (Fs)
8	Cumulus-under-stratocumulus (Cu-under-Sc)
*	Sky-obscuring fog (fog)

* With present weather code ww = 10–12 or 40–49.

2. Data

a. OWS cloud type observations

Synoptic cloud type observations from the surface are particularly useful for studying low cloudiness because human observers identify clouds by morphological type, which is qualitatively related to the dynamical and thermodynamical environment in which the clouds occur. Table 1 lists synoptic code numbers (World Meteorological Organization 1975) and informal names of low cloud types examined in this study. Occasionally it is not possible to observe low cloudiness due to sky-obscuring fog (diagnosed by the present-weather code), which is identified as an additional ''low cloud type'' for the purposes of this paper. OWS data provide synoptic observations of cloudiness every 3 h (with occasional missing data) during January 1945–December 1987 for OWS C (52.75°N, 35.5°W) and August 1943–April 1974 for OWS N (30°N, 140°W). However, the present study used only observations since December 1951 for OWS C and April 1954 for OWS N because the VOS dataset begins in December 1951 and OWS N changed locations in March 1954.

b. VOS meteorological observations

Surface meteorological observations were obtained from a preliminary version of the Extended Edited Cloud Report Archive (EECRA), an updated version of the Edited Cloud Report Archive (Hahn et al. 1996).[1] The EECRA is a collection of individual synoptic surface cloud observations with coincident meteorological observations obtained from the Comprehensive Ocean–

[1] This preliminary version of the EECRA was also the source for the low cloud type climatologies presented in Norris (1998b).

TABLE 2. Number of dates used in the composites, effective sample size, number of VOS observations used to calculate divergence, mean divergence, and mean NCEP 700-mb ω with 95% confidence interval.

	Number of dates	Effective sample size	Number of VOS observations	VOS divergence (10^{-6} s^{-1})	NCEP 700-mb ω (mb day^{-1})
JJA OWS C C_L 0	279	150	998	2.0	-23 ± 10
JJA OWS C C_L 2	251	130	966	1.7	34 ± 12
JJA OWS C C_L 5	1447	613	5398	3.3	14 ± 5
JJA OWS C C_L 6	341	184	1183	-0.9	-8 ± 8
JJA OWS C C_L 7	233	140	1091	-5.7	-95 ± 14
JJA OWS C C_L 8	313	153	1468	1.1	23 ± 10
JJA OWS C FOG	402	204	1385	-1.5	-24 ± 7
DJF OWS C C_L 2	565	327	1369	-0.2	34 ± 11
DJF OWS C C_L 5	568	338	1111	7.4	14 ± 14
DJF OWS C C_L 7	232	153	539	-6.3	-173 ± 25
DJF OWS C C_L 8	103	71	260	6.9	34 ± 21
JJA OWS N C_L 1	133	78	632	2.7	34 ± 9
JJA OWS N C_L 2	336	192	1565	0.7	26 ± 6
JJA OWS N C_L 5	636	291	2824	2.5	24 ± 5
JJA OWS N C_L 8	1702	711	9041	1.6	27 ± 3
DJF OWS N C_L 1	108	72	563	4.8	59 ± 21
DJF OWS N C_L 2	364	204	1545	-0.9	25 ± 14
DJF OWS N C_L 5	716	350	3256	2.8	10 ± 9
DJF OWS N C_L 8	549	312	2975	0.4	-2 ± 10

Atmosphere Data Set (Woodruff et al. 1987). VOS observations of wind and SST are known to suffer from various problems (e.g., Cardone et al. 1990; Isemer and Hasse 1991; Kent et al. 1993; Ramage 1987; Saur 1963; Tabata 1978), but no attempt was made to correct the data since it is unlikely that any biases would vary with the low cloud type observed by the OWS.

c. NCEP analyses

The NCEP–NCAR reanalysis project uses a frozen global assimilation system and atmospheric general circulation model to assimilate historical raw observations into dynamically consistent and completely sampled data. This advantage, however, comes at the cost of relying on the model and assimilation procedure, which can be particularly influential in the boundary layer. Since the NCEP model uses ship-reported winds primarily to obtain the rotational part of the flow (J. Derber 1998, personal communication), the analyzed surface divergence is often problematic (e.g., frequent convergence under much of the subtropical anticyclone). Analyzed vertical motion above the boundary layer is more realistic, at least when there is strong synoptic forcing, but instantaneous values can suffer from substantial temporal noise (e.g., Fig. 8 of Bretherton et al. 1995). Results from both VOS observations and NCEP analyses will be presented since they provide a complimentary view of the true synoptic environment; VOS composites are free from model errors, and NCEP composites are dynamically consistent.

Analyses of SLP, 1000-mb wind, and 700-mb ω interpolated onto a regular 2.5° lat $\times$ 2.5° long grid with smoothing and truncation at T36 were available for 0000, 0600, 1200, and 1800 UTC. Values for 0300, 0900, 1500, and 2100 UTC were calculated by linearly interpolating in time at each grid point. Vertical motion was examined at the 700-mb level because it is near to but rarely inside the MBL. Results for the 500-mb and 850-mb levels are similar and hence will not be shown.

3. Compositing procedure

a. Selection of dates

Regional composites of surface wind, SLP, and SST were constructed by averaging all VOS observations reported on dates and times of day when the same low cloud type was observed at the OWS. Similar composites of 1000-mb wind, SLP, and 700-mb ω were constructed from the analyses. Dates were selected only if the cloud type had also been recorded in the reports from 3 h before and after the observation. Furthermore, because surface observers sometimes have difficulty identifying clouds on dark nights (Hahn et al. 1995; Norris 1998a; Rozendaal et al. 1995), sufficient illumination according to the criterion of Hahn et al. (1995) was required 3 h before, 3 h after, and at the time of the observation. This causes a daytime bias in the composites, but attempting to uniformly sample the diurnal cycle using only good-illumination cloud reports would greatly decrease the sample size. Table 2 lists the number of dates contributing to each low cloud type regional composite at OWS C and N during the seasons of June–August (JJA) and December–February (DJF).

b. Averaging

VOS observations of SLP, SST, and the zonal and meridional wind components reported on the composite dates and times of day for a low cloud type were averaged into 2° lat $\times$ 4° long grid boxes in the North

Atlantic and the North Pacific. Because the EECRA includes OWS observations that are not always flagged, observations near OWS locations were excluded from the analysis. This will prevent the high density of OWS observations relative to VOS observations from biasing the 2° × 4° means. Area-weighted means at 4° lat × 8° long were constructed from the 2° × 4° means to reduce biases resulting from nonuniform sampling. Because VOS observations alone incompletely sample the wind field on a given date, divergence from the raw observations was calculated from the composite wind field instead of compositing divergence calculated from instantaneous wind fields.

NCEP analyses of SLP, 1000-mb zonal and meridional wind components, and 700-mb ω on the composite dates and times of day were averaged retaining the same 2.5° × 2.5° grid resolution. Smoothing and truncation at T36 gives the analyses approximately the same resolution in latitude as the 4° × 8° VOS averages.

c. Calculation of statistical significance

Since VOS observations do not provide data at regular locations for all composite dates and times of day, statistical significance can be calculated only for the NCEP composites. One important consideration is the effective sample size since many of the contributing dates and times of day occur within a few hours of each other. Observations separated by time τ are effectively independent if the lag correlation for time τ is less than $\exp(-2)$ (Leith 1973). Applying this method to the time series of 700-mb ω at the OWS locations indicates observations at OWS C and OWS N during JJA are independent if separated by 15 h and observations at OWS C and OWS N during DJF are independent if separated by 12 h. These criteria were applied to the lists of composite dates and times of day to obtain the effective sample sizes for each (listed in Table 2). Temporally dependent data are still allowed to contribute to a composite, but the reduced number of degrees of freedom will be used in the calculation of statistical significance.

4. Results

a. Local vertical motion

Figure 1 displays distributions of instantaneous local ω at 700 mb associated with various low cloud types at OWS C during JJA. These distributions were obtained by linearly interpolating nearby NCEP 2.5° × 2.5° values to the location of OWS C for each composite date and time of day. Table 2 records the mean vertical velocity for each cloud type along with its 95% confidence interval using the effective sample size and a two-sided *t* test. It is likely that noise in the analyses (e.g., Bretherton et al. 1995) substantially contributes to the large scatter apparent in the distributions. With only 6-h instantaneous values available it is difficult to quantify

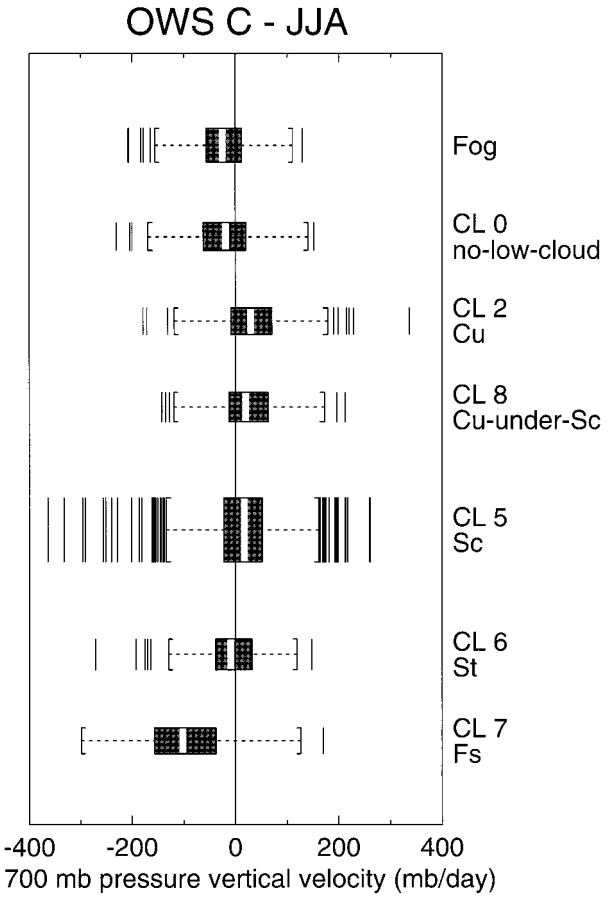

FIG. 1. Distributions of instantaneous 700-mb ω for various low cloud types at OWS C during JJA, displayed as boxplots. The white bar shows the median value; the shaded box contains the inner quartiles; the whiskers extend to 1.5 times the interquartile range or the limits of the data (whichever is closer); outliers are beyond. The height of the box is proportional to the square root of the number of dates contributing to the composite.

the magnitude of the spurious variability, but the present results can be considered as an upper bound to the true variability. Figure 1 shows that stratocumulus and cumulus types (C_L 5, 8, 2) usually occur with subsidence and the other types (C_L 7, 6, 0, and sky-obscuring fog) usually occur with ascent. Mean values of ω for each cloud type are significantly different from the others except for the following pairs: C_L 0 and C_L 6, C_L 0 and sky-obscuring fog, C_L 8 and C_L 5, C_L 8 and C_L 2 (Table 2). Nonetheless, there is much overlap between distributions of vertical motion for cloud types besides bad-weather stratus (C_L 7). This illustrates that other processes, such as horizontal advection, also have a role in distinguishing cloud type.

b. North Atlantic climatology

To provide a foundation for examining the synoptic environments associated with various low cloud types, climatological (1952–87) SLP, surface wind, diver-

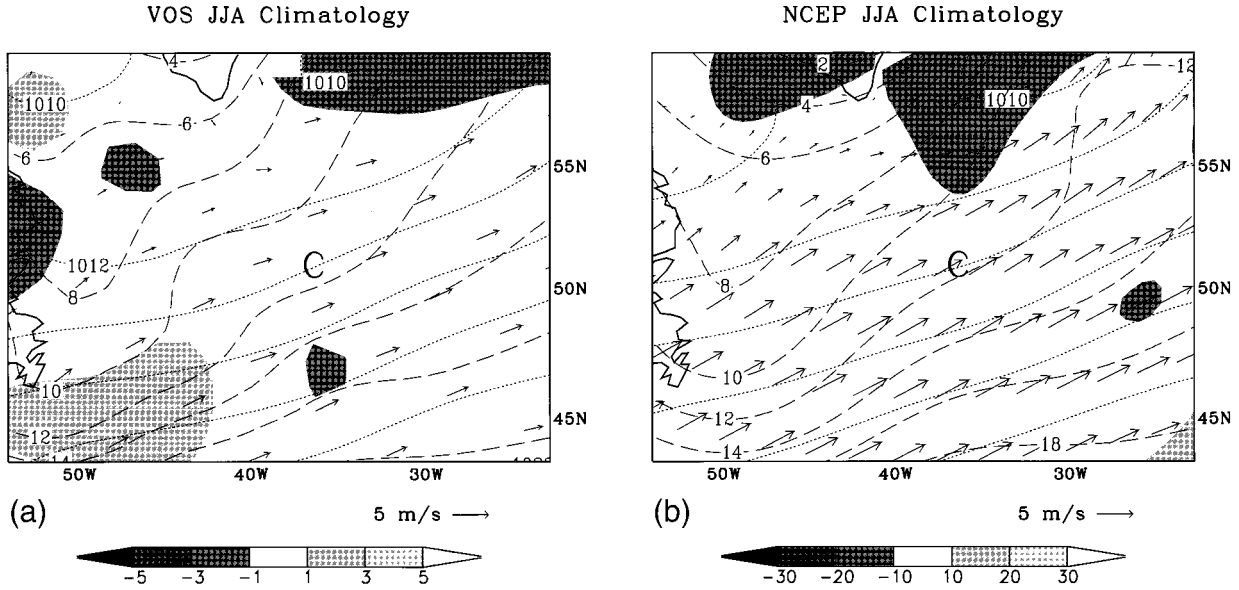

FIG. 2. (a) VOS climatological surface wind (arrows), SLP (dotted), SST (dashed), and calculated divergence (shading) for the region around OWS C during JJA. Contour intervals are 2°C for SST and 2 mb for SLP; divergence units are 10^{-6} s^{-1}; wind vectors and shading intervals are as indicated at the bottom of the figure. (b) NCEP climatological 1000-mb wind (arrows), SLP (dotted), SST (dashed), and 700-mb ω (shading). Contour intervals as in (a); vertical velocity units are mb day^{-1}.

gence, and SST over the western midlatitude North Atlantic during JJA from good-illumination VOS observations are presented in Fig. 2a. Climatological SLP, 1000-mb wind, 700-mb ω, and surface temperature (prescribed SST over the ocean) from the NCEP analyses are presented in Fig. 2b. The coast of Newfoundland is on the western border, the southern tip of Greenland is on the northern border, and OWS C is at the center of the plots. Although the arrows in Fig. 2a indicate the mean surface wind over most of the region is southwesterly at 3 m s^{-1}, considerable synoptic variation occurs and the typical surface wind speed is about 7 m s^{-1}. Accordingly, composites for low cloud types associated with a specific synoptic environment will exhibit strong wind vectors distinctly different from the climatology. Likewise, composites for low cloud types associated with a variety of meteorological conditions will exhibit weak wind vectors tending to resemble the climatology. Mean divergence and vertical velocity in the vicinity of OWS C is near zero, and the close alignment of wind vectors with SST contours indicates mean advection over the SST gradient in the vicinity of OWS C is also near zero.

c. Clouds not under capping inversions

Figure 3a shows VOS composite SLP, surface wind, and divergence associated with bad-weather stratus (C_L 7) at OWS C during JJA. The number of dates used in the composite and the value of and number of observations used to calculate divergence at OWS C are recorded in Table 2. Figure 3b shows NCEP composite SLP, 1000-mb wind, and 700-mb ω. Bad-weather stratus typically occurs in a region of strong surface convergence and above-surface ascent slightly ahead of an advancing trough and low center. Winds in the vicinity of OWS C have a large southerly component, implying warm advection. The DJF bad-weather stratus composites (not shown) also display strong surface convergence and southerly flow associated with a surface trough and low center. These results are consistent with near-saturated conditions through most of the troposphere and positive air–sea temperature differences for bad-weather stratus [Fig. 5 and Table 4 of Norris (1998a)]. They are also in agreement with the study of Lau and Crane (1997), who found that nimbostratus reported by surface observers was most frequent east of a surface low center in a region of strong southerly flow at the surface and upward motion in the midtroposphere.

VOS and NCEP composites for fair-weather stratus (C_L 6) are displayed in Fig. 4. The VOS composite suggests a tendency for fair-weather stratus to occur with weak convergence associated with an extratropical cyclone. The NCEP composite does not have closed SLP contours but does show ascent ahead of a surface trough. Weak surface convergence and ascent is consistent with the occurrence of fair-weather stratus in a saturated and stably stratified layer with frequent drizzle at OWS C (Fig. 5 of Norris 1998a). Considering that the composites are similar to the climatologies, particularly in the southern half of the plots, it is likely that clouds that surface observers identify as fair-weather stratus are produced by a variety of meteorological conditions.

Norris (1998a) found that meteorological conditions

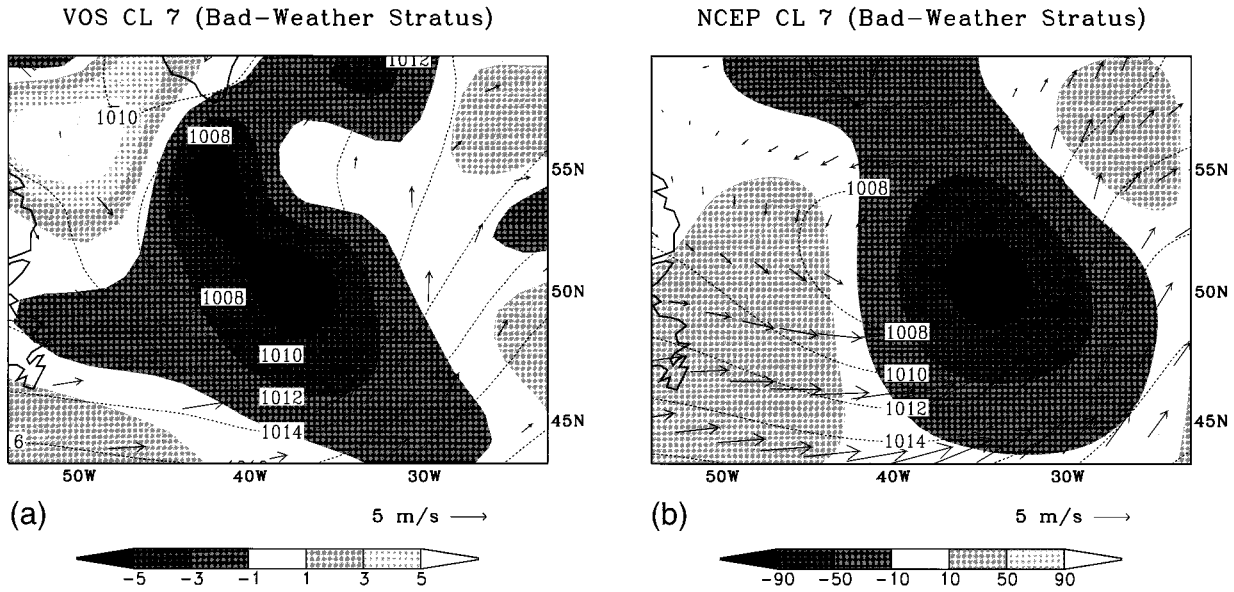

FIG. 3. (a) VOS composite surface wind (arrows), SLP (dotted), and calculated divergence (shading) associated with bad-weather stratus (C_L 7) at OWS C during JJA. Contour intervals are 2 mb for SLP; divergence units are 10^{-6} s^{-1}; wind vectors and shading intervals are as indicated at lower right of the figure. (b) NCEP composite 1000-mb wind (arrows), SLP (dotted), and 700-mb ω (shading) associated with bad-weather stratus (C_L 7) at OWS C during JJA. Contour intervals are 2 mb for SLP; vertical velocity units are mb day^{-1}; wind vectors and shading intervals are as indicated at lower right of the figure.

associated with sky-obscuring fog and no-low-cloud (C_L 0) were similar, except for the large difference in low-level relative humidity. Both cloud types occur with a surface-based inversion and a positive air–sea temperature difference, implying warm advection. VOS and NCEP composites for sky-obscuring fog (Fig. 5) and no-low-cloud (Fig. 6) show that these cloud types typically occur with southwesterly flow. Mean NCEP 1000-mb advection over the climatological SST gradient at OWS C is 2.2 ± 0.4[2] °C day^{-1} for sky-obscuring fog and 1.4 ± 0.4[2] °C day^{-1} for no-low-cloud. In addition to advection rate, the two cloud types differ according

[2] Two-tail 95% confidence interval.

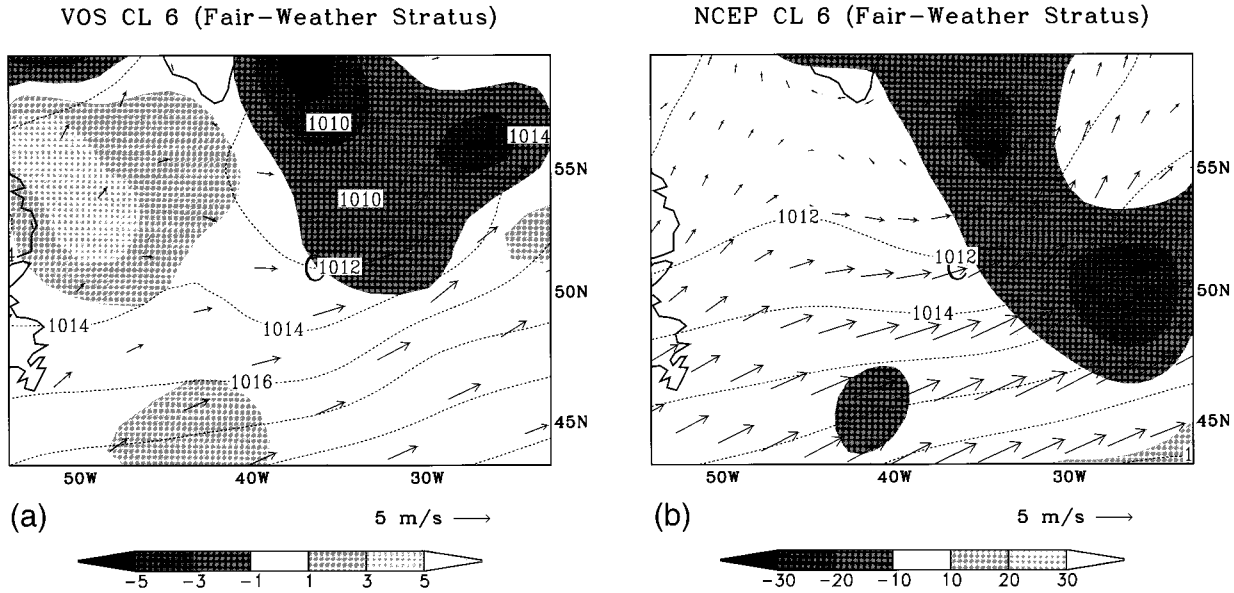

FIG. 4. (a) As in Fig. 3a except for fair-weather stratus (C_L 6). (b) As in Fig. 3b except for fair-weather stratus (C_L 6) and a different shading interval.

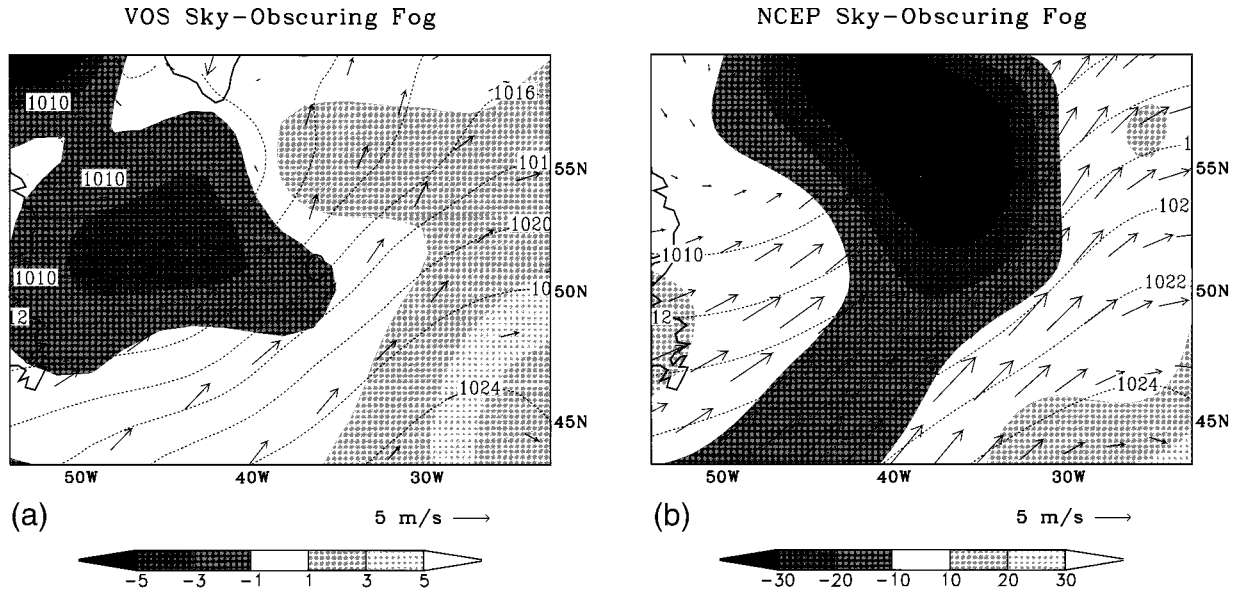

FIG. 5. (a) As in Fig. 4a except for sky-obscuring fog. (b) As in Fig. 4b except for sky-obscuring fog.

to the presence of surface convergence in the case of fog and surface divergence in the case of no-low-cloud (Figs. 5a and 6a). Sky-obscuring fog appears to occur as surface convergence begins in the warm sector of an approaching extratropical cyclone. Lau and Crane (1997) found similar results for fogs that accompany wintertime cyclones. It is not surprising no-low-cloud typically occurs with surface divergence and advection of air over colder water since the most favorable conditions for a cloudless MBL over the open ocean are continuous entrainment of dry air forced by subsidence and scant upward moisture flux due to positive stratification near the surface. Less difference between sky-obscuring fog and no-low-cloud is apparent in the NCEP composites. Both composites show ascent at 700 mb (Figs. 5b and 6b), suggesting that the divergence associated with no-low-cloud occurs in a very shallow layer.

d. Clouds under capping inversions

Composites for ordinary stratocumulus (C_L 5) show surface divergence, subsidence, and weak ridging (Fig. 7), consistent with previous aircraft studies (e.g., Boers

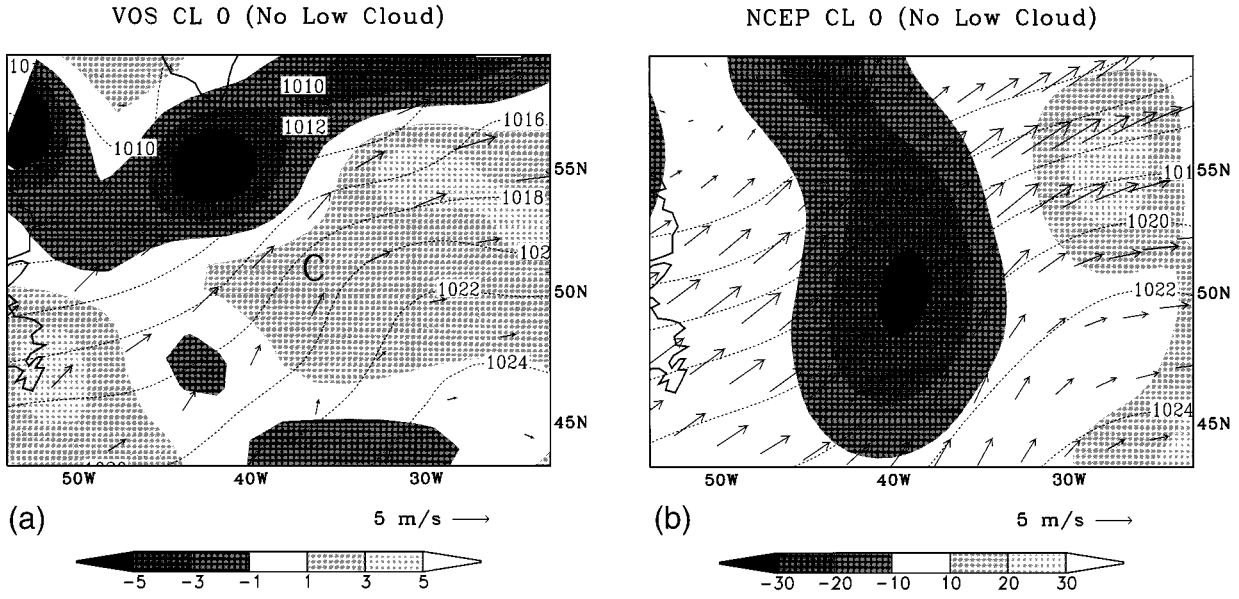

FIG. 6. (a) As in Fig. 4a except for no-low-cloud (C_L 0). (b) As in Fig. 4b except for no-low-cloud (C_L 0).

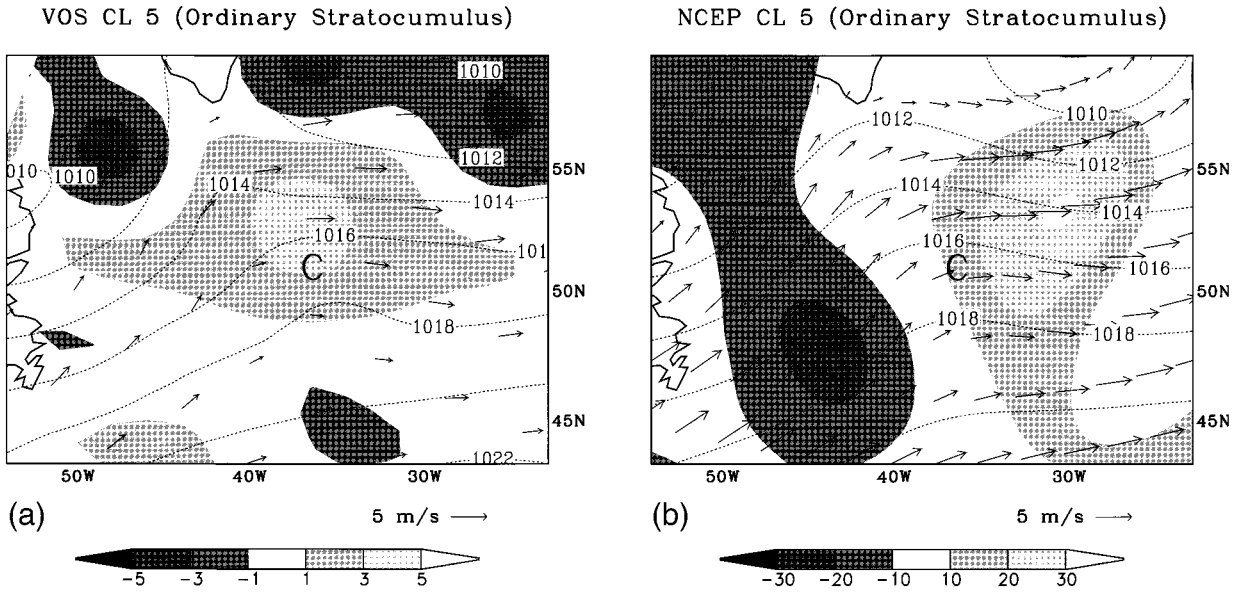

FIG. 7. (a) As in Fig. 4a except for ordinary stratocumulus (C_L 5). (b) As in Fig. 4b except for ordinary stratocumulus (C_L 5).

et al. 1996; Slingo et al. 1982). As is the case for fair-weather stratus (Fig. 4), the composites for ordinary stratocumulus resemble the climatology. Thus, it appears that the primary large-scale parameter distinguishing the two cloud types may be the direction of vertical motion. In addition to the direct effect of divergence or convergence on subsidence drying in the MBL, subsidence may influence cloud type by drying the atmosphere above the MBL, thus promoting greater radiative cooling at the MBL cloud top. Consistent with this supposition, less upper-level cloud amount is observed for stratocumulus than for stratus (not shown), suggesting that the turbulence generated by cloud top radiative cooling is greater for stratocumulus than for fair-weather stratus. The difference in sign of vertical motion is consistent with the occurrence of stratocumulus in a convectively well-mixed MBL under a strong inversion and the occurrence of fair-weather stratus in a stably stratified saturated MBL [Figs. 3 and 5 of Norris (1998a)].

It should be noted that in addition to the simultaneous subsidence indicated in Fig. 7, the MBL may have experienced greater subsidence in the recent past. For example, trajectory analysis performed by Boers et al. (1998a) for a case of stratocumulus observed at the ridge axis of a midlatitude anticyclone indicates that the MBL air had experienced greater divergence in the 15–20 h prior to arriving at the ridge axis. Moreover, because the speed of the synoptic wave is greater than that of the MBL wind (Boers et al. 1998a), the trajectory does not follow the wind field such as that displayed in Fig. 7 but instead comes from higher latitudes.

Composites for cumulus-under-stratocumulus (C_L 8) and moderate and large cumulus (C_L 2) are displayed in Figs. 8 and 9. These cloud types often form in regions of divergence and equatorward and westerly flow to the west of surface troughs and low centers (e.g., Boers and Krummel 1998; Boers et al. 1997; Boers et al. 1998b; Lau and Crane 1997; Martin et al. 1997; Nichols 1984). The pattern for moderate and large cumulus is especially strong (Fig. 9), indicating it rarely occurs except in the cold sector of extratropical cyclones. Divergence is weaker for cumulus and cumulus-under-stratocumulus than for stratocumulus (Table 2 and Fig. 10a), implying weaker subsidence at the top of the MBL. All other things being equal, weaker subsidence will act to produce deeper MBLs for cumulus and cumulus-under-stratocumulus than for stratocumulus (Fig. 4 of Norris 1998a). Cumulus also occurs with greater surface buoyancy than cumulus-under-stratocumulus (Smith and Jonas 1995).

Composites constructed for ordinary stratocumulus, cumulus-under-stratocumulus, and moderate and large cumulus at OWS C during DJF (not shown) largely duplicate those for JJA. Values for surface divergence and 700-mb ω at OWS C during DJF are listed in Table 2. As was the case for JJA, divergence is stronger for stratocumulus than for cumulus (Fig. 10a). This is consistent with the much shallower MBL observed at OWS C during DJF for stratocumulus than for cumulus (Fig. 4 of Norris 1998a). Divergence for cumulus-under-stratocumulus during DJF is not shown in Fig. 10a because Table 2 indicates there are probably not enough observations available for a reliable calculation (note the small number of dates contributing to the composite).

To examine the role of surface divergence in the eastern subtropical ocean, composites were constructed for ordinary stratocumulus, cumulus-under-stratocumulus, moderate and large cumulus, and small cumulus at OWS N during JJA and DJF. Maps are not displayed for the sake of conciseness. Unlike the midlatitude North At-

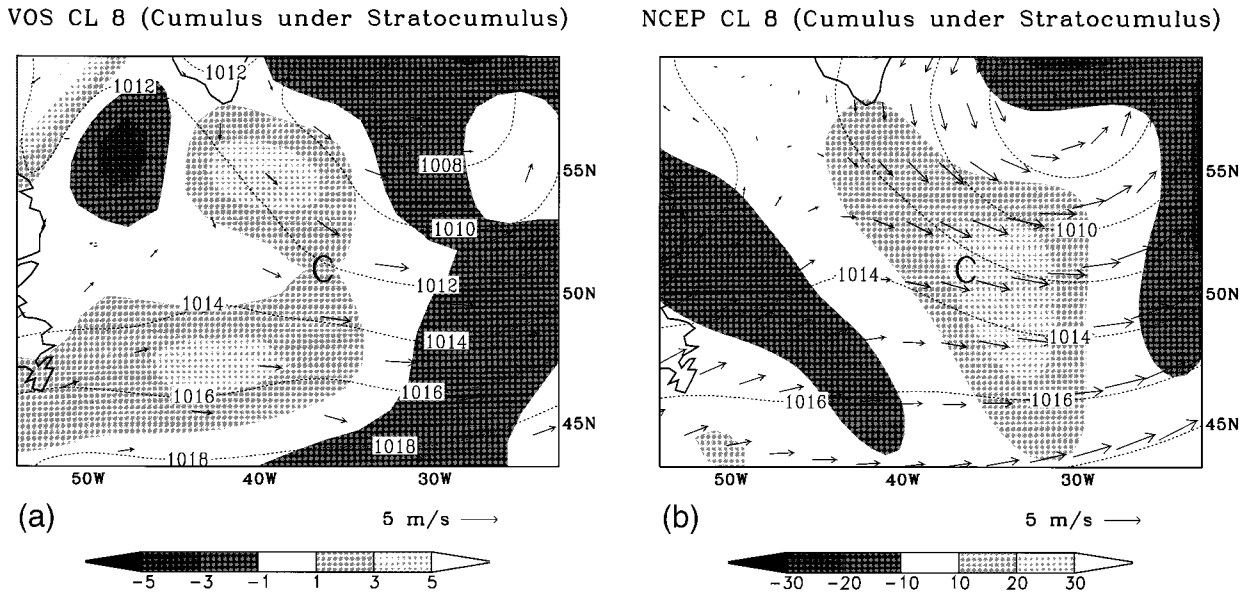

FIG. 8. (a) As in Fig. 4a except for cumulus-under-stratocumulus (C_L 8). (b) As in Fig. 4b except for cumulus-under-stratocumulus (C_L 8).

lantic, the summertime eastern subtropical North Pacific has little synoptic variability due to the dominance of the subtropical anticyclone. Accordingly, the JJA composites tend to resemble each other except in the SLP pattern; cloud type changes from stratocumulus to cumulus-under-stratocumulus to moderate and large cumulus to small cumulus as the subtropical anticyclone progressively weakens and is located farther west. During DJF, cloud type changes from stratocumulus to cumulus under stratocumulus to moderate and large cumulus to small cumulus as the subtropical anticyclone progressively weakens and is located farther east. Values for surface divergence and 700-mb ω at OWS N during JJA and DJF are listed in Table 2.

Figure 10a shows that divergence values at OWS N increase from moderate and large cumulus to cumulus-under-stratocumulus to stratocumulus during both JJA and DJF. However, the strongest divergence is observed to occur with small cumulus. This does not contradict the positive correlation between divergence and low cloud amount found by Klein (1997) because small cumulus infrequently occurs at OWS N (Fig. 2 of Norris 1998a). The surface wind speed associated with small cumulus is significantly lower than wind associated with

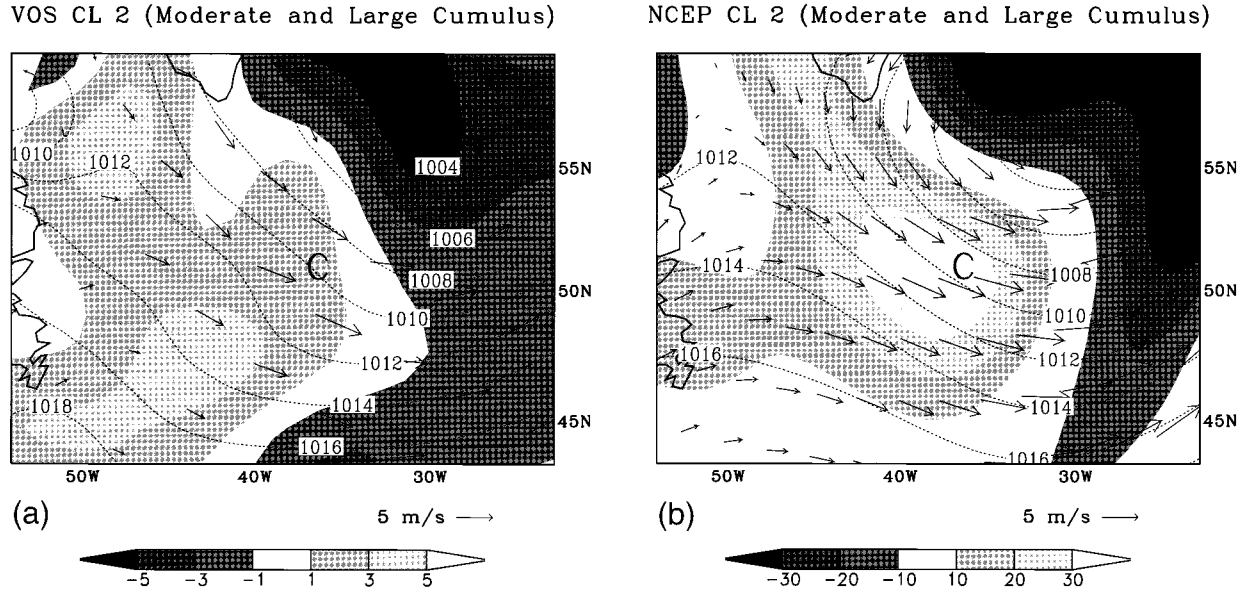

FIG. 9. (a) As in Fig. 4a except for moderate and large cumulus (C_L 2). (b) As in Fig. 4b except for moderate and large cumulus (C_L 2).

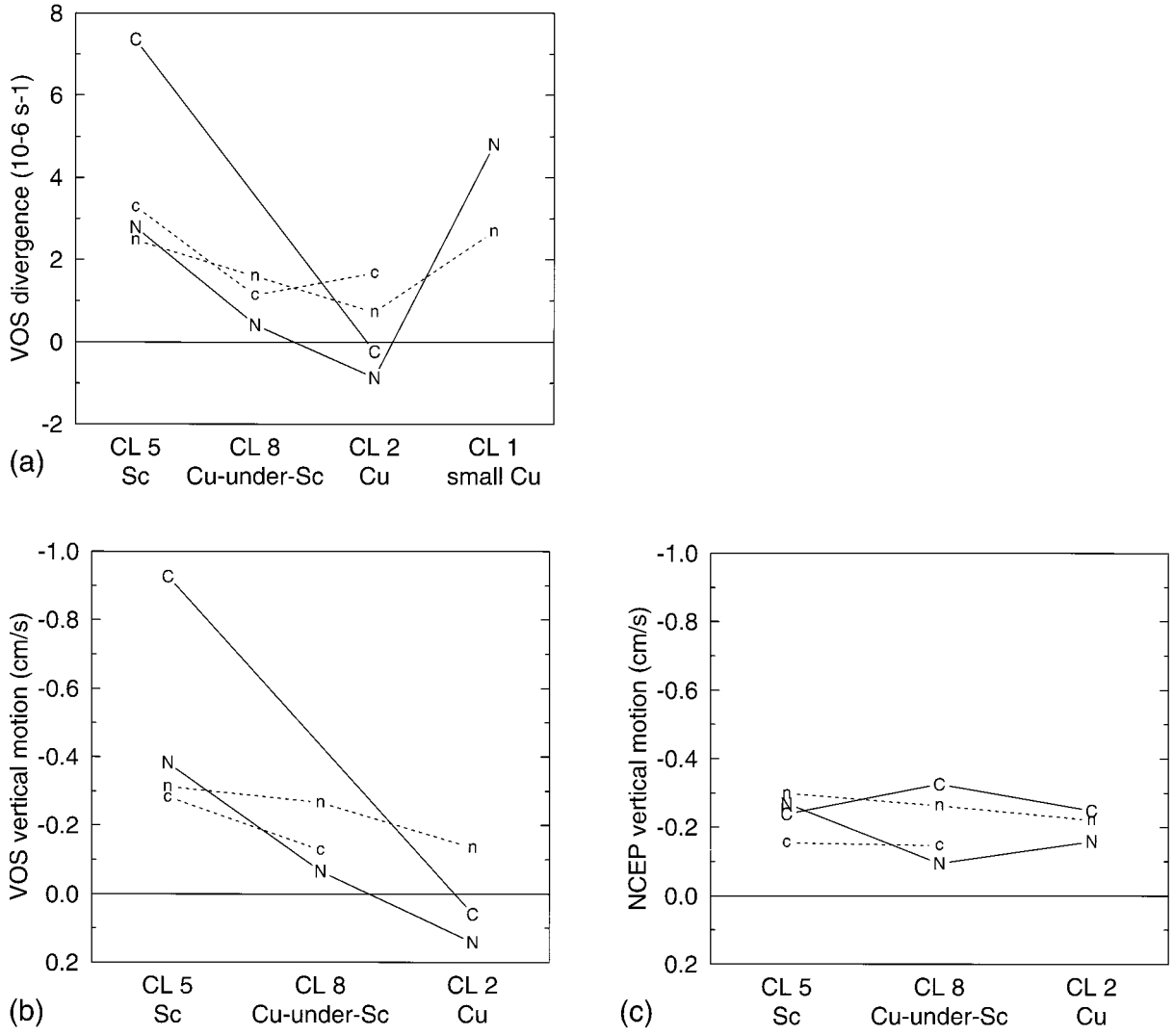

FIG. 10. Composite values of (a) VOS divergence, (b) estimated VOS top-of-MBL vertical velocity, and (c) interpolated NCEP top-of-MBL vertical velocity at OWS locations for ordinary stratocumulus (C_L 5), cumulus-under stratocumulus (C_L 8), moderate and large cumulus (C_L 2), and small cumulus (C_L 1). OWS locations are identified by letter for DJF (uppercase and solid lines) and JJA (lowercase and dotted lines).

the other cloud types during JJA. However, without more information it is difficult to determine if the difference in wind speed or other factors leads to the formation of small cumulus instead of stratocumulus when subsidence is strong.

If it is assumed that divergence is constant within the MBL, vertical velocity at the top of the MBL is the product of the surface divergence and the MBL height. Figure 10b shows estimated vertical velocity for moderate and large cumulus, cumulus-under-stratocumulus, and ordinary stratocumulus at OWS C and OWS N using values of surface divergence from Table 2 and values of MBL height from Table 3 of Norris (1998a). At both OWS during JJA and DJF, the subsidence rate is greatest for stratocumulus, less for cumulus-under-stratocumulus, and least for moderate and large cumulus. Because there were not enough contributing soundings to calculate MBL height for moderate and large cumulus at OWS C during JJA and small cumulus at OWS N, these were left out of Table 3 of Norris (1998a) and are left out of Fig. 10b. Note that small cumulus must occur in a relatively shallow MBL, otherwise they would be called moderate or large cumulus. The few available soundings suggest they probably occur in MBLs with about the same height and therefore approximately the same subsidence rate as stratocumulus MBLs.

Figure 10c displays NCEP vertical velocity obtained by linearly interpolating in pressure ω at 700, 850, and 925 mb to the MBL height used in the VOS calculation. Unlike the VOS estimates, NCEP vertical velocities show no trend or large variation between cloud types. Given the obvious problems with NCEP surface diver-

gence and the possible sensitivity of NCEP vertical motion to the model boundary layer parameterization, it is questionable whether the directly calculated NCEP values are more reliable than the VOS estimates. In any case, note that both the estimated and directly calculated subsidence rates for stratocumulus and cumulus-under-stratocumulus at OWS N during JJA ($\sim$0.3 cm s^{-1}) are only slightly less than the value obtained by Betts and Ridgway (1988) for subsidence driven by radiative cooling ($\sim$0.04 Pa s^{-1} or $\sim$0.4 cm s^{-1}).

5. Conclusions

Regional composites of SLP, wind, surface divergence calculated from raw observations, and 700-mb ω from NCEP analyses were constructed for low cloud types observed at OWS C in the western midlatitude North Atlantic during summer. They show physically consistent relationships between low cloud type and the regional surface synoptic environment. Bad-weather stratus typically occurs with southerly flow, strong surface convergence, and strong ascent slightly ahead of a surface trough and low center. Mean southwesterly flow over decreasing SST is associated with sky-obscuring fog and no-low-cloud. Although both cloud types occur with slight ascent at 700 mb, sky-obscuring fog occurs with surface convergence and strong warm advection and no-low-cloud with surface divergence and less strong warm advection. Moderate and large cumulus and cumulus-under-stratocumulus occur with mean northwesterly flow and divergence in the cold sector of an extratropical cyclone. Composites for ordinary stratocumulus and fair-weather stratus tend to resemble the climatology, indicating they are produced by a variety of meteorological conditions. Both occur with mean westerly flow, but fair-weather stratus is associated with weak convergence, weak ascent, and a surface trough whereas ordinary stratocumulus is associated with divergence, subsidence, and a surface ridge.

This magnitude and sign of divergence in the MBL is an important large-scale parameter affecting low cloud type and therefore low cloud amount and other cloud properties. In fact, the composites at OWS C during JJA suggest it may be a primary parameter distinguishing sky-obscuring fog from no-low-cloud and fair-weather stratus from stratocumulus. Furthermore, an examination of divergence and estimated top-of-MBL subsidence at OWS C and OWS N during DJF and JJA indicates a strong tendency for ordinary stratocumulus to occur with the strongest divergence and subsidence, cumulus-under-stratocumulus with less divergence and subsidence, and moderate and large cumulus with the least (and sometimes slightly negative) divergence and subsidence. Subsidence rates obtained by interpolating NCEP ω to the top of the MBL are much more uniform between different cloud types and different locations, but this disparate behavior may be caused by problems in the model assimilation procedure and boundary layer parameterization. If the subsidence rates estimated from the raw observations are indeed more reliable, the fact that the same relative relationship is observed at a midlatitude location and a subtropical location during both summer and winter suggests it generally occurs over the global ocean. If so, decreasing subsidence, in addition to increasing SST (Krueger et al. 1995; Wyant et al. 1997), may promote the transition from stratocumulus to trade cumulus in low-latitude oceans.

Acknowledgments. This work was supported by the National Science Foundation while Joel Norris was an Advanced Study Program postdoctoral fellow at the National Center for Atmospheric Research. Preliminary work was supported by an Earth Observing System grant, NASA Grant NAGW-2633, while Joel Norris was a graduate student at the University of Washington. OWS data were obtained from the National Climatic Data Center (NCDC) in Asheville, North Carolina. NCEP analyses were obtained from Chi-Fan Shih in the NCAR Data Support Section. The authors wish to thank Gabriel Lau, Philip Rasch, Robert Pincus, Brian Soden, Bjorn Stevens, and an anonymous reviewer for useful comments.

REFERENCES

Albrecht, B. A., D. A. Randall, and S. Nicholls, 1988: Observations of marine stratocumulus clouds during FIRE. *Bull. Amer. Meteor. Soc.*, **69,** 618–626.

——, C. S. Bretherton, D. Johnson, W. H. Schubert, and A. S. Frisch, 1995: The Atlantic Stratocumulus Transition Experiment—ASTEX. *Bull. Amer. Meteor. Soc.,* **76,** 889–904.

Betts, A. K., and W. Ridgway, 1988: Coupling of radiative, convective, and surface fluxes over the equatorial Pacific. *J. Atmos. Sci.,* **45,** 522–536.

Boers, R., and P. B. Krummel, 1998: Microphysical properties of boundary layer clouds over the Southern Ocean during ACE 1. *J. Geophys. Res.,* **103,** 16 651–16 663.

——, J. B. Jensen, P. B. Krummel, and H. Gerber, 1996: Microphysical and short-wave radiative structure of wintertime stratocumulus clouds over the Southern Ocean. *Quart. J. Roy. Meteor. Soc.,* **122,** 1307–1339.

——, ——, and ——, 1997: A line of convection embedded in a stratocumulus-topped boundary layer. *Quart. J. Roy. Meteor. Soc.,* **123,** 207–221.

——, P. B. Krummel, S. T. Siems, and G. D. Hess, 1998a: Thermodynamic structure and entrainment of stratocumulus over the Southern Ocean. *J. Geophys. Res.,* **103,** 16 637–16 650.

——, J. B. Jensen, and P. B. Krummel, 1998b: Microphysical and short-wave radiative structure of stratocumulus clouds over the Southern Ocean: Summer results and seasonal differences. *Quart. J. Roy. Meteor. Soc.,* **124,** 151–168.

Bretherton, C. S., P. Austin, and S. T. Siems, 1995: Cloudiness and marine boundary layer dynamics in the ASTEX Lagrangian experiments. Part II: Cloudiness, drizzle, surface fluxes, and entrainment. *J. Atmos. Sci.,* **52,** 2724–2735.

Cardone, V. J., J. G. Greenwood, and M. A. Cane, 1990: On trends in historical marine wind data. *J. Climate,* **3,** 113–127.

——, ——, and ——, 1995: The effect of moonlight on observation of cloud cover at night, and application to cloud climatology. *J. Climate,* **8,** 1429–1446.

——, ——, and ——, 1996: Edited synoptic cloud reports from ships and land stations over the globe, 1982–1991. Rep #NDP026B,

45 pp. [Available from Carbon Dioxide Information Analysis Center, Oak Ridge National Laboratory, P.O. Box 2008, Oak Ridge, TN 37831-6050.]

Isemer, H.-J., and L. Hasse, 1991: The scientific equivalent scale: Effects on wind statistics and climatological air–sea flux estimates in the North Atlantic Ocean. *J. Climate,* **4,** 819–836.

Kalnay, E., and Coauthors, 1996: The NCEP/NCAR 40-Year Reanalysis Project. *Bull. Amer. Meteor. Soc.,* **77,** 437–471.

Kent, E. C., P. K. Taylor, B. S. Truscott, and J. S. Hopkins, 1993: The accuracy of voluntary observing ships' meteorological observations—Results of the VSOP-NA. *J. Atmos. Oceanic Technol.,* **10,** 591–608.

Klein, S. A., 1997: Synoptic variability of low-cloud properties and meteorological parameters in the subtropical trade wind boundary layer. *J. Climate,* **10,** 2018–2039.

——, and D. L. Hartmann, 1993: The seasonal cycle of low stratiform clouds. *J. Climate,* **6,** 1587–1606.

——, ——, and J. R. Norris, 1995: On the relationships among low cloud structure, sea surface temperature, and atmospheric circulation in the summertime northeast Pacific. *J. Climate,* **8,** 1140–1155.

Krueger, S. K., G. T. McLean, and Q. Fu, 1995: Numerical simulation of the stratus-to-cumulus transition in subtropical marine boundary layer. Part I: Boundary-layer structure. *J. Atmos. Sci.,* **52,** 2839–2850.

Lau, N.-C., and M. W. Crane, 1997: Comparing satellite and surface observations of cloud patterns in synoptic-scale circulation systems. *Mon. Wea. Rev.,* **125,** 3172–3189.

Leith, C. E., 1973: The standard error of time-average estimates of climatic means. *J. Appl. Meteor.,* **12,** 1066–1069.

Martin, G. M., D. W. Johnson, P. R. Jonas, D. P. Rogers, I. M. Brooks, and R. W. Barlow, 1997: Effects of airmass type on the interaction between warm stratocumulus and underlying cumulus clouds in the marine boundary-layer. *Quart. J. Roy. Meteor. Soc.,* **123,** 849–882.

Nicholls, S., 1984: The dynamics of stratocumulus: Aircraft observations and comparisons with a mixed layer model. *Quart. J. Roy. Meteor. Soc.,* **110,** 783–820.

——, and J. Leighton, 1986: An observational study of the structure of stratiform cloud sheets. Part I: Structure. *Quart. J. Roy. Meteor. Soc.,* **112,** 431–460.

Norris, J. R., 1998a: Low cloud type over the ocean from surface observations. Part I: Relationship to surface meteorology and the vertical distribution of temperature and moisture. *J. Climate,* **11,** 369–382.

——, 1998b: Low cloud type over the ocean from surface observations. Part II: Geographical and seasonal variations. *J. Climate,* **11,** 383–403.

——, Y. Zhang, and J. M. Wallace, 1998: Role of low clouds in summertime atmosphere–ocean interactions over the North Pacific. *J. Climate,* **11,** 2482–2490.

Ramage, C. S., 1987: Secular change in reported surface wind speeds over the ocean. *J. Climate Appl. Meteor.,* **26,** 525–528.

Rozendaal, M. A., C. B. Leovy, and S. A. Klein, 1995: An observational study of diurnal variations of marine stratiform cloud. *J. Climate,* **8,** 1795–1809.

Saur, J. F. T., 1963: A study of the quality of sea water temperatures reported in logs of ships' weather observations. *J. Appl. Meteor.,* **2,** 417–425.

Slingo, A., 1990: Sensitivity of the earth's radiation budget to changes in low clouds. *Nature,* **343,** 49–51.

——, S. Nicholls, and J. Schmetz, 1982: Aircraft observations of marine stratocumulus during JASIN. *Quart. J. Roy. Meteor. Soc.,* **108,** 833–856.

Smith, S. A., and P. R. Jonas, 1995: Observations of the turbulent fluxes in fields of cumulus clouds. *Quart. J. Roy. Meteor. Soc.,* **121,** 1185–1208.

Tabata, S., 1978: Comparison of observations of sea surface temperatures at Ocean Station P and NOAA buoy stations and those made by merchant ships traveling in their vicinities, in the northeast Pacific Ocean. *J. Appl. Meteor.,* **17,** 374–385.

Weaver, C. P., and V. Ramanathan, 1997: Relationships between large-scale vertical velocity, static stability, and cloud radiative forcing over Northern Hemisphere extratropical oceans. *J. Climate,* **10,** 2871–2887.

Woodruff, S. D., R. J. Slutz, R. L. Jenne, and P. M. Steurer, 1987: A comprehensive ocean–atmosphere data set. *Bull. Amer. Meteor. Soc.,* **68,** 1239–1250.

World Meteorological Organization, 1975: International cloud atlas. Vol. I. WMO Publ. 407, WMO, 155 pp.

Wyant, M. C., C. S. Bretherton, H. A. Rand, and D. E. Stevens, 1997: Numerical simulations and a conceptual model of the stratocumulus to trade cumulus transition. *J. Atmos. Sci.,* **54,** 168–192.